Development of a model for flexural rigidity of fishing net with a spring mass approach and its inverse identification by metaheuristic parametric optimization.

Vincent Benoit [1, *], Di Cesare Noëlie [2], Simon Julien

[1] IFREMER-STH/LTBH, Station de Lorient, 8 rue François Toullec, 56100, Lorient, France
[2] Univ. Bretagne-Sud, UMR CNRS 6027, IRDL, F-56100, Lorient, France

* Corresponding author : Benoit Vincent, email address : benoit.vincent@ifremer.fr

Abstract :

The assessment of mesh resistance to opening is a key factor when coming to fishing gear design to study or optimize the fishing selectivity process. Different authors proposed methodologies to achieve twine flexural rigidity identification and mesh opening angle at rest. Their experimental protocols could rely on complex installations and instrumentation, and identification needs dedicated models or software with possible important set up time. Sometimes, different flexural rigidity and rest angle values for a given netting type were proposed depending on identification or experimental conditions, leading to difficulties to choose a value for implementation in netting structures simulation software. The new methodology proposed in this article is based on a simplified experimental protocol taking plasticity into account and an identification method derived from an end user dedicated software, to determine mechanical and dimensional characteristics of common netting materials. Identified flexural rigidity and rest angle values fall inside the interval provided by authors using similar methods. Identified parameters have been used to predict the geometry of two T90 netting cylinders with errors lower than 3%.

Highlights

► Selectivity of fishing nets can be improved through the modeling of their shape. ► Netting shape and tension are highly dependent on parameters like twine flexural rigidity. ► A new netting twine flexural 3D model is proposed and implemented in a proven algorithm. ► An experimental protocol including plasticity and identification method are used to identify parameters. ► Identified flexural rigidity and rest mesh angle are coherent with literature results for common nettings. ► Applied to larger netting structures, model and experimentation differ by 3%.

1 Introduction

The reform of the European Common Fisheries Policy (CFP) of 2013 has increased the pressure on fishers, compelling them to reduce the catch of untargeted species. A technical way to avoid fishing untargeted species is to improve the selection capability of the fishing gear. For fishing gear like trawls made of nettings, mechanical properties of braided twines have a strong influence on net meshes opening (Herrmann et al., (2013)) and consequently on the selectivity properties, especially in the terminal part of the fishing gear: the codend is pulled into a bulb-shape as it is loaded by fish, which provides more open meshes in the front part of the bulb which enables the fish to escape (Robertson and Stewart, (1988)).

The mesh opening mechanism is complex and involves the twine bending stiffness. A direct measurement of bending stiffness is not possible and needs an inverse identification process where a set of mesh characteristics, including bending stiffness, is adjusted till the model best reproduces a series of experiments. Experimental protocols and numerical modeling are involved in this process.

Several experimental protocols have been tested by different authors to assess the value of the bending stiffness of twine composing fishing nets. Sala et al., (2007) developed a complex and expensive experimental system to measure the forces needed to uniformly deform a sample of netting. Bending stiffness could be deduced using the beam theory. Priour and Cognard, (2011) proposed to measure the deformation of a vertical netting sample under different loads and the flexion of a netting sample as a cantilever under its own weight. De La Prada and González, (2016) proposed a way to establish a relation between the height of a netting sample and the force applied in its lower part in a vertically suspended and uniaxial configuration using a tensile test bench. Morvan et al., (2016) used a similar configuration where each lower node of the netting sample had its own weight to simulate a force, with no need of a tensile test bench. The sample heights were measured for the different loads but the sample width was not considered to identify the bending stiffness.

De La Prada and González, (2016) state that axial rigidity (EA) for common netting twines ranges between 500N and 3000N and that its effect on netting deformation is negligible compared to flexural deformations, except for deformations that hardly happen in real marine applications. In parallel, the theory used by O'Neill, (2002) does not involve axial elasticity and value of axial rigidity are not provided by Morvan et al., (2016) .

Mechanical and geometrical properties of netting samples can be identified by the optimization of a set of parameters used in a physical oriented approach model. Priour, (2001); Priour and Cognard, (2011) modeled the flexural rigidity with a torque located at the physical knot supposing that the twines remain straight. De La Prada and González, (2016) used two different approaches: (1) asymptotic development of a model of the twine as a bi-dimensional double-clamped beam developed by O'Neill. This model was based on the beam bending equations under several hypothesis: (i) the bending moment is proportional to the twine curvature and (ii) no axial elasticity. (2) A finite element model allows the assessment of the force – displacement response, then fitting techniques have been used to set bi-dimensional dimensionless models that compare accurately ("spline" model) and reasonably accurately (polynomial model, 5% to 10% of deviation), with the exact solution previously

given by O'Neil. These models express the reaction force as an explicit function of the twine deformation and can be used to solve large deformations of the net. These models assume uniform deformations and are not applicable to 3 dimensional problems. A finite element model in Abaqus for a small number of meshes have been developed by Morvan et al. Mesh sides are assumed to behave like Timoshenko beams, taking into account the mesh resistance to the net's opening, allowing the simulation of non-uniform deformation. Again, the optimization does not consider the relation between the sample width and the load. The length of the physical knots is not considered. These models are specifically designed to identify netting mechanical properties. Thus, the identification of netting mechanical parameters by the final user of the netting modelling software can be difficult. In this context, this work proposes to apply identification results to larger structures simulation, by comparing the numerical and experimental results.

Nettings used in fishing gear can be loaded with high forces able to generate permanent plastic deformations in twines and knots (De La Prada, (2014)). Plasticity has been taken into consideration in De La Prada and Gonzalez, (2015) in a single load/unload cycle. For each load the operator waited until the sample length becomes stable. Moreover, the maximum force (leading to stretch the sample to 80% of its maximum stretched length) was applied during one hour after the last load increment and before the first unload increment. The relations between sample height and forces for the load and the unload phases were then analyzed separately. Plasticity was not taken into consideration by Morvan et al., (2016).

In the present work, we attempt to establish a practical methodology to estimate the mechanical and geometrical properties of netting materials. The proposed method is original as it is based on the use of artificially intelligent algorithms applied to the algorithm used in netting structure simulation in marine environment. This netting structure simulation algorithm is implemented in a widely used commercial software (DynamiT) specialized in trawl simulation presented by Nguyen et al., (2015); Nguyen and Winger, (2016) and thus does not rely on any other theory nor software. Moreover, it is proposed to overcome some of the drawbacks of previous methods: (1) the present method considers eventual flexural forces and deformations normal to the two normalized netting directions N and T (Fig. 1), (2) the simple experimental protocol proposed by De La Prada and Gonzalez, (2015) was slightly simplified to enable the end users to identify by themselves the properties of nettings without the need of laboratory facilities, (3) the plasticity is taken into account in a more realistic way, (4) identified parameters for some common nettings are applied to larger netting structures simulation and compared to experimental results. Finally, an original metaheuristic optimization algorithm based on artificial intelligence is used to identify the constitutive parameters of the fishing net model.

2 Fishing net mechanical modelling

2.1 Modelling of meshes

In the present work, netting is modelled by using the work of Bessonneau and Marichal, (1998) and Le Bris and Marichal, (1999) where an axial elasticity model has been added for the present work. Net meshes are considered as twines and nodes. Each twine, or mesh side, can be split into two or more rigid bars to model its suppleness. Thus, a mesh is broken down in a set of mass nodes linked by rigid bars supporting a tension. Additional forces are added to model gravity forces or any external force (Fig. 1).
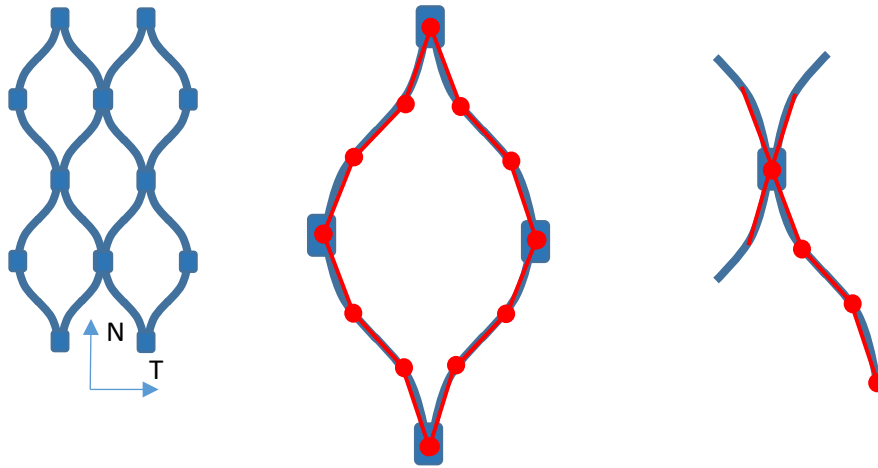

Fig. 1 : a net is split into elementary meshes which are split again in a set of rigid bars. Normalized netting directions N and T denote the knot direction (Normal) and the Transverse direction.

2.2 Dynamical equilibrium of netting elements

Let's consider a system constituted by *N* nodes and *M* rigid bars. The mass of a bar is concentrated at each end nodes. Forces applied on bars (weights and internal forces for instance) are located at end nodes. Bessonneau and Marichal proposed a method to solve the dynamic equilibrium of this system using the second law of Newton applied to each node in a Galilean frame. If we consider the bar *j* linked to the node *i*, then half the mass of the bar *j* and half the external forces applied on bar *j*, are assumed to be applied directly on node *i*. Thus N equations can be written as follows:

$$m_i \vec{\gamma}_i = \sum_{neigbourbars\ j} \left(\vec{T}_{ij} + \vec{H}_{ij} \right) \quad i \in [1, N] \quad [1]$$

where m_i is the pseudo mass of node *i* taking into account half masses of bars *j*, $\vec{\gamma}_i$ is its acceleration, $\vec{T}_{ij}$ is the tension applied by neighbor bars *j* on node *i* and $\vec{H}_{ij}$ is half an external force applied to bar *j*.

The so called length condition is imposed by solving the following equation where ℓ_{kl} is the length of the bar limited by nodes *k* and *l* :

$$\ell_{kl}^{\,2} = \left(\vec{X}_k - \vec{X}_l\right)^2 \quad [2]$$

where $\vec{X}_k$ is the position of node *k* in a Galilean frame.

Using a simple semi implicit first order Euler scheme for velocity to express the velocity of node *k* at time *n+1* using the know time step *h, it follows*:

$$h\,\vec{V}_k^{\,n+1} = \vec{X}_k^{\,n+1} - \vec{X}_k^{\,n} \quad [3]$$

We get an explicit expression for velocity from eq. [2]:

$$\left(\vec{V}_k^{\,n+1} - \vec{V}_l^{\,n+1}\right)\left(\vec{X}_k^{\,n} - \vec{X}_l^{\,n}\right) = \frac{1}{2h}\ell_{kl0}^{\,2} - \frac{1}{2h}\left(\vec{X}_k^{\,n} - \vec{X}_l^{\,n}\right)^2 \quad [4]$$

Using again an Euler scheme for acceleration in eq. [1] and substituting velocities in eq. [4] we get a linear equation for each structure bar, where bar tensions are the unknown variables to be solved

$$\left(\vec{X}_k^{\,n} - \vec{X}_l^{\,n}\right)^2 + h^2\left(\vec{V}_k^{\,n} - \vec{V}_l^{\,n}\right)^2 + 2h\left(\vec{X}_k^{\,n} - \vec{X}_l^{\,n}\right)\left(\vec{V}_k^{\,n} - \vec{V}_l^{\,n}\right)$$

$$+ 2h^2\left(\vec{X}_k^{\,n} - \vec{X}_l^{\,n}\right)\left(\frac{1}{M_k}\left\{\sum_{p \in NB(k)} T_{jp}^{\,n+1}\frac{\vec{X}_p^{\,n} - \vec{X}_k^{\,n}}{\ell_{jn}} + \vec{H}_{kp}^{\,n}\right\}\right) \qquad [5]$$

$$+ 2h^2\left(\vec{X}_k^{\,n} - \vec{X}_l^{\,n}\right)\left(\frac{1}{M_l}\left\{\sum_{p \in NB(l)} T_{lp}^{\,n+1}\frac{\vec{X}_p^{\,n} - \vec{X}_l^{\,n}}{\ell_{in}} + \vec{H}_{lp}^{\,n}\right\}\right) = \ell_{kl}^{\,2}$$

where NB(k) is the set of neighbor bars of the node *k*, ℓ_{kp} is the length of bar B_{kp} .

The matrix equation for T is symmetrical and is efficiently solved with Gauss method for law rank matrix (lower than 1000 unknown variables) and by considering conjugate gradient methods for higher ranks.

Bessonneau and Marichal and later LeBris have used the following algorithm to solve this system of stiff equations in the time domain: from initial positions and velocities verifying the length conditions, external forces are calculated, tensions are solved from the linear equation [5]. Acceleration, velocities and positions are calculated at the time step n+1. This iteration is repeated until a convergence criterion is reached. This algorithm has been used in this work to solve internal forces and positions of the netting twine and nodes.

2.3 External forces

The application considered in this study only requires weight forces due to the material specific weight and punctual weights applied in some structure nodes. Damping force due to hydrodynamic load is not considered.

2.3.1 Weight

Twine weight forming mesh bars and netting knots is applied to calculation nodes. Weights attached to the lower part of the netting model are applied to the lower nodes of the model.

2.4 Internal forces

2.4.1 Axial elasticity

In order to have a more realistic modeling and to increase the diagonal dominance of the matrix equation, a linear axial elasticity term has been added in equation [2].

$$\ell_{kl} = \ell_{0kl}\left(1 + k_{kl}T_{kl}\right) \qquad [6]$$

Where k_{kl} is the inverse of the bar axial stiffness and the length of bar free of load ℓ_{0kl} . These length conditions are linearized, assuming kT << 1, which means that relative axial elongation of a mesh side is low, which is verified in most cases of practical use of fishing nets application.

Length condition at time n+1 becomes:

$$\ell_{kl}^{n+1^2} = \ell_{0kl}^{2}\left(1 + 2k_{kl}T_{kl}^{n+1}\right) = \left(\vec{X}_k^{n+1} - \vec{X}_l^{n+1}\right)^2 \qquad [2b]$$

We get a new explicit expression for velocity from eq. [6]

$$\left(\vec{V}_k^{n+1} - \vec{V}_l^{n+1}\right)\left(\vec{X}_k^{n} - \vec{X}_l^{n}\right) = \frac{1}{2h}\left(1 + 2k_{kl}T_{kl}^{n+1}\right)\ell_{kl0}^{2} - \frac{1}{2h}\left(\vec{X}_k^{n} - \vec{X}_l^{n}\right)^2 \qquad [8]$$

This leads to a new set of matrix equations

$$\left(\vec{X}_k^{n} - \vec{X}_l^{n}\right)^2 + h^2\left(\vec{V}_k^{n} - \vec{V}_l^{n}\right)^2 + 2h\left(\vec{X}_k^{n} - \vec{X}_l^{n}\right)\left(\vec{V}_k^{n} - \vec{V}_l^{n}\right)$$

$$+ 2h^2\left(\vec{X}_k^{n} - \vec{X}_l^{n}\right)\left(\frac{1}{M_k}\left\{\sum_{p\in NB(k)} T_{jp}^{n+1}\frac{\vec{X}_p^{n} - \vec{X}_k^{n}}{\ell_{jn}} + \vec{H}_{kp}^{n}\right\}\right) \qquad [9]$$

$$+ 2h^2\left(\vec{X}_k^{n} - \vec{X}_l^{n}\right)\left(\frac{1}{M_l}\left\{\sum_{p\in NB(l)} T_{lp}^{n+1}\frac{\vec{X}_p^{n} - \vec{X}_l^{n}}{\ell_{in}} + \vec{H}_{lp}^{n}\right\}\right) = \left(1 + 2k_{kl}T_{kl}^{n+1}\right)\ell_{kl}^{2}$$

where the dominance of the diagonal is increased with elasticity terms making it easier to solve.

Coefficient *k* can be elongation-dependent depending on the material constituting the netting. Other authors chose to neglect the axial rigidity or concluded that this parameter has negligible effects for standard marine applications. To feed the proposed model with this parameter, the knot deformation when loading a mesh side is then taken into account. The assumption is made that the knot behavior is not depending on the twine. Wanchana et al., (2002) has established a linear load–elongation curve resulting from breaking strength tests by considering the "English knot" for PE twines. The relative knot strength is 65% of the tensile breaking strength and the elongation at breaking is 22.8%. A first approximation of the k coefficient in equation [2b] is thus $k = \frac{0.228}{0.65 \, Bs}$ where Bs is the tensile breaking strength in Newton. The breaking load of the 3mm twine used in this work is 120 kgw, which leads to 1/k=3356 N. The breaking load of 4mm PE twine is 180 kgw, which leads to 1/k=5034 N.

2.4.2   Flexural forces

The connected structure made of bars as described above is not a representative model of an actual net as it does not take into account the twines flexural resistance. According to elementary beam theory, the relationship between the applied bending moment M and the resulting curvature of the center line of the beam is given by:

$$-\frac{EI}{\rho} = M$$

where ρ is the radius of curvature, E is the elastic modulus, I is the inertia of the beam's section. The expression of the bending moment is valid under the assumption of a symmetrical beam and if its transverse sections remain normal to the bended centerline. Thus, the bending moment is assumed to be proportional to the curvature of the twine at each location of the twine, the bending stiffness is EI also known as the flexural rigidity. For present work and like authors cited in this work, the same assumptions are made, leading to good results.

Flexural rigidity of twines is taken into account to model its resistance to bending in these two situations: (1) to model the suppleness of the twine and (2) when the twine is embedded into a netting node.

2.4.2.1   Curvature radius to model the suppleness of a twine

In Fig. 2, the green line is supposed to be a bended netting twine. The bar B_{ki} defined by its two ends nodes $\overrightarrow{N_k N_i}$ and the bar B_{ij} defined by $\overrightarrow{N_i N_j}$ are two adjacent bars discretizing the bended twine element.
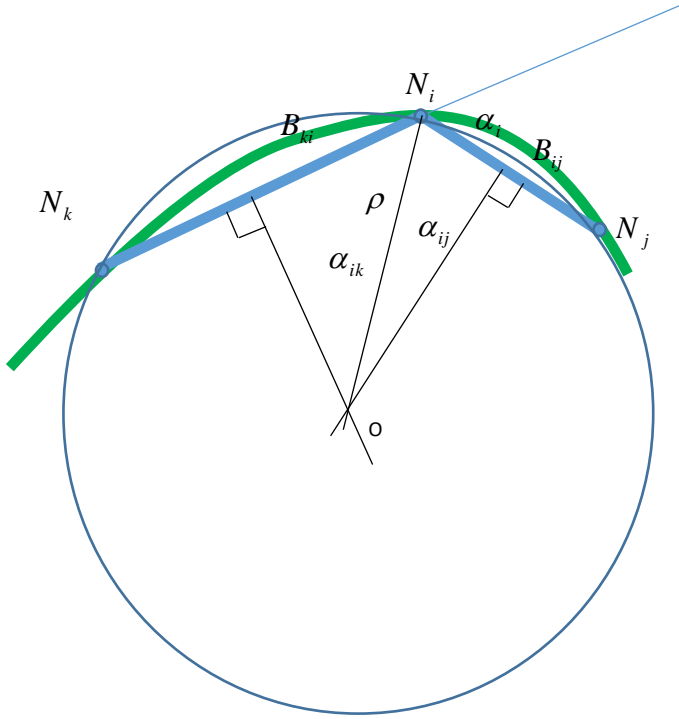
Fig. 2: discretization of 2 adjacent bars (blue) to model the bending moment of a twine (green curve).

The rotation angle of the discrete bar $\overrightarrow{N_i N_j}$ from its non-bended position is α_i. The radius of curvature ρ is assumed to be the radius of the osculating circle to the local twine shape. The circle is the circumcircle to the triangle (Ni Nj Nk). Thus its center is located at the intersection of the bisectors to (Ni Nj) and (Nj Nk). Consequently, α_i is also the angle between the bisectors. Thus, it follows:

$$\sin(\alpha_{ik}) = \frac{\ell_{ik}}{2\rho} \text{ and } \sin(\alpha_{ij}) = \frac{\ell_{ij}}{2\rho}$$

By using $\alpha_i = \alpha_{ik} + \alpha_{ij}$ and the common relation

$$\sin(\alpha_1) + \sin(\alpha_2) = 2\sin\left(\frac{\alpha_1 + \alpha_2}{2}\right)\cos\left(\frac{\alpha_1 - \alpha_2}{2}\right)$$

it comes $\rho = \dfrac{\ell_{ij} + \ell_{ik}}{4\sin\left(\dfrac{\alpha_i}{2}\right)}$ and $M_i = -EI \dfrac{4\sin\left(\dfrac{\alpha_i}{2}\right)}{\ell_{ij} + \ell_{ik}}$

A general expression using triangle points co-ordinates to calculate the radius of the circumcircle of a triangle could also be used.
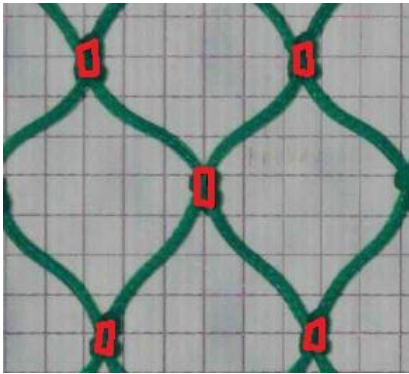
Fig. 3 : piece of netting: knots underlined in red cannot be considered as points.

The observation of a piece of netting shows that knots cannot be considered as punctual objects (Fig. 3). They have an extension in the netting normal direction. Consequently, it is proposed to model netting knots with a bar as shown in Fig. 4. Observation also show that twines are not embedded in knots with a null angle between two adjacent twines.

In order to define the angle of twine free of load, we define a local referential linked to the knot (Fig. 4).
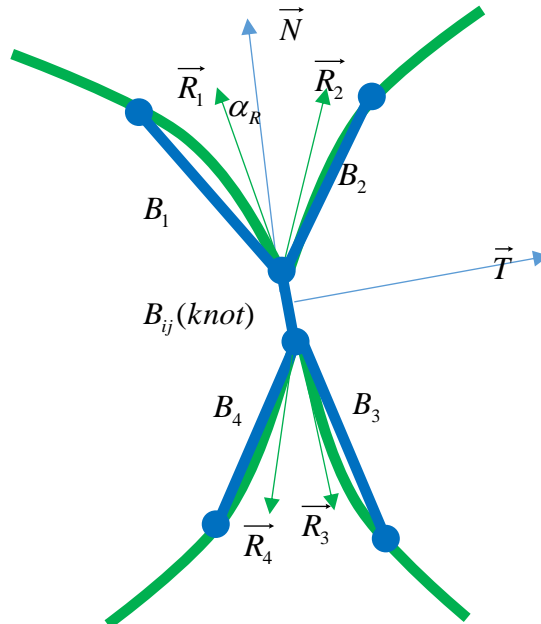

Fig. 4 : local numbering and referential to define the orientation of bars. Green lines denotes actual twines and blue lines denote modeled lines.

The local orthonormal referential is defined by vectors $\vec{N}$ and $\vec{T}$. $\vec{N}$ is aligned with the so-called normal direction of the netting, which defines the orientation of netting nodes. $\vec{N}$ is simply defined

by the bar B_{ij} and is normalized. Vector $\vec{T}$ is first approximately defined with

$$\vec{t} = normalised \; (\vec{B_2} + \vec{B_3} - \vec{B_1} - \vec{B_4})$$ where $\vec{B_i}$ is the vector oriented from the central node to the

other end of bar B_i, and the normalization function is defined by $normalised \, (\vec{u}) = \dfrac{\vec{u}}{\left\|\vec{u}\right\|}$. All $\vec{B_i}$ have

the same length in this application.

Vector $\vec{t}$ is a unit vector close to $\vec{T}$ but that does not ensure orthogonality with $\vec{N}$. Using $\vec{n} = \vec{t} \wedge \vec{N}$ defining a unit vector normal to the average mesh plan, $\vec{T} = \vec{n} \wedge \vec{N}$ can be calculated which is normal to $\vec{N}$. Thus ($\vec{N}$, $\vec{T}$) defines a local orthonormal system to the node and is used to define the rest position of bars linked to this node.

Vectors $\vec{R_i}$ denote the rest orientation of bar i. Assuming the rest angle α_R is known and a knot and its 4 bars are symmetrical at rest, $\vec{R_i}$ is simply calculated as follows:

$$\vec{R_1} = -\sin \alpha_R \vec{T} + \cos \alpha_R \vec{N}$$

$$\vec{R_2} = \sin \alpha_R \vec{T} + \cos \alpha_R \vec{N}$$

$$\vec{R_3} = -\vec{R_1}$$

$$\vec{R_4} = -\vec{R_2}$$

The shape of the bended twine embedded in knot B_{ij} is supposed to be approached by the circle tangent to $\vec{R_k}$ at the node N_i and passing through the node N_k (Fig. 5). We obtain the following expression of the radius of curvature:

$$\rho = \frac{\ell_{ik}}{2\sin(\alpha_i)} \quad \text{and} \quad M_i = -EI \; \frac{2\sin(\alpha_i)}{\ell_{ik}}$$
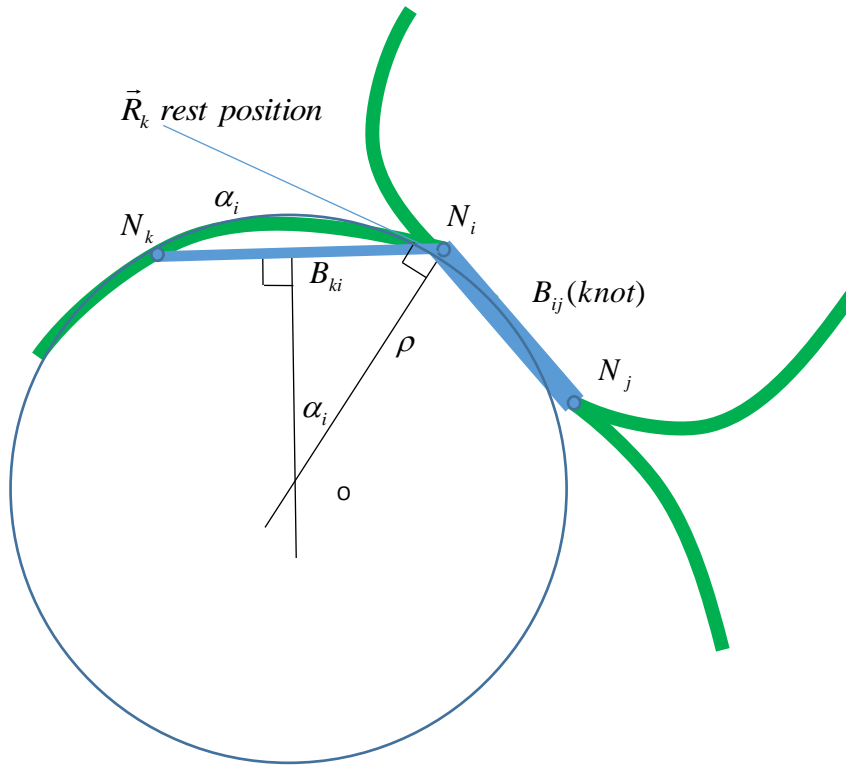
Fig. 5 : assessment of the curvature of a twine embedded in a knot. $\vec{R}_k$ is not aligned with B_{ij} , we consider the circle tangent to $\vec{R}_k$ and passing through N_k and N_i. Green lines denote actual twines and blue lines bars model twines or knots.

We assume that angles and moments are positive when turning counterclockwise on Fig. 2 Fig. 4 and Fig. 5 . Then $M_{ij} < 0$ is the moment applied on B_{ki} by B_{ij} and $-M_{ij} > 0$ is the moment applied on B_{ij} by B_{ki} .

2.4.3   Tridimensional Implementation

Explanations given from Fig. 2-6 are valid for a 2D sketch. When considering 3D models, bending moments are applied on each bar by the mean of forces normal to the plan defined by the two bars (Fig. 6).

For instance, the bending moment M applied by bar B_{ki} on bar B_{ij} is $M = F_{ij}\ell_{ij}$ where ℓ_{ij} is the length of bar B_{ij}. Force $F_{ij} = \dfrac{M}{\ell_{ij}}$ is applied on node N_j and $-F_{ij}$ is applied on node N_i to keep the resultant of forces applied on the bar B_{ij} constant.
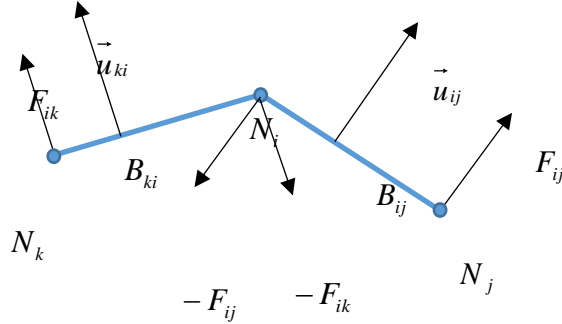

Fig. 6 : forces applied on bars to implement bending moments

Forces applied on B_{ij} and on B_{ki} have then to be calculated. These forces are coplanar to (B_{ki}, B_{ij}) as no torsion moment is assumed.

We need to calculate a unit vector having the same direction and orientation of the force. Let's call $\vec{u}_{ij}$ the unit vector normal to B_{ij}, coplanar to (B_{ki}, B_{ij}), being oriented so that $\overrightarrow{N_k N_i} \cdot \vec{u}_{ij} > 0$

and $\vec{u}_{ki}$ is the unit vector normal to B_{ki}, coplanar to (B_{ki}, B_{ij}), being oriented so that $\overrightarrow{N_j N_i} \cdot \vec{u}_{ki} > 0$

The unit vector normal to (B_{ki}, B_{ij}) is defined as follows:

$$\vec{m}_{ijk} = \frac{\overrightarrow{N_j N_i} \wedge \overrightarrow{N_k N_i}}{\left\| \overrightarrow{N_j N_i} \wedge \overrightarrow{N_k N_i} \right\|}$$

If $\overrightarrow{N_j N_i}$ and $\overrightarrow{N_k N_i}$ are collinear, the bending moment is zero.

The unit vectors supporting the forces applied on B_{ki} and B_{ij} can be calculated with:

$$\vec{u}_{ij} = \vec{m}_{ijk} \wedge \frac{\overrightarrow{N_j N_i}}{\left\| \overrightarrow{N_j N_i} \right\|} \quad \text{and} \quad \vec{u}_{ik} = -\vec{m}_{ijk} \wedge \frac{\overrightarrow{N_k N_i}}{\left\| \overrightarrow{N_k N_i} \right\|}$$

Forces applied to model the bending torque are calculated from the moment $\vec{M} = \vec{d} \wedge \vec{F}$ where $\vec{d}$ is the so-called moment arm. Using the relation of the double cross product:

$\vec{u} \wedge (\vec{v} \wedge \vec{w}) = (\vec{u}.\vec{w})\vec{v} - (\vec{u}.\vec{v})\vec{w}$, we get

$$\vec{F} = -\frac{\vec{d} \wedge \vec{M}}{d^2}$$

Consequently, forces to implement are:

$$\overline{M}_i = -EI \frac{4\sin\left(\dfrac{\alpha_i}{2}\right)}{\ell_{ij} + \ell_{ik}} \vec{m}_{ijk} \quad \text{for modelling twine bending force, which leads to:}$$

$$\vec{F}_i = EI \ \frac{4\sin\left(\dfrac{\alpha_i}{2}\right)}{\ell\left(\ell_{ij} + \ell_{ik}\right)} \vec{u}_{ij}$$

$$\overrightarrow{M}_i = -EI \frac{2\sin(\alpha_i)}{\ell_{ik}} \vec{m}_{ijk} \quad \text{for modelling embedded twine bending, which leads to:}$$

$$\overrightarrow{F}_i = EI \frac{2\sin(\alpha_i)}{\ell \ell_{ik}} \vec{u}_{ij}$$

With ℓ is denoting the bar length where the force torque is applied.

3   Determination of the physical properties of the netting model by inverse identification

3.1   Particle Swarm Optimization algorithm

In the Particle Swarm Optimization (PSO) algorithm (J. Kennedy;R. Eberhart, (1995); Reynolds, (1987)), particles are defined that represent, each, a potential solution to the optimization problem to be solved. These particles are defined in the solution domain by a position, noted **X**, and their speed[1], noted **V**. They are then flying smartly through the solution domain, by following each other to finally converge together to the global minimum of the considered objective function. The speed and the position of particle *i* are then re-calculated at each iteration *t+1* of the optimization process, as follows:

$$V_i^{t+1} = \omega \times V_i^t + c_1 \times r_1 \times \left(P_{i,best}^t - X_i^t\right) + c_2 \times r_2 \times \left(G_{best}^t - X_i^t\right)$$
$$X_i^{t+1} = X_i^t + V_i^{t+1}$$

where $P_{i,best}^t$ is the personal best position of particle *i* found so far, given in terms of a position in the solution domain, G_{best}^t is the global best position found so far by the swarm. ω is an inertia, that is the influence of the previous speed on the calculation of the new one, c_1 and c_2 are confident parameters, weighing the influence of the entire swarm versus the personal memory of the particle, r_1 and r_2 are random parameters defined in $[0;1]$. ω is balancing the abilities of the algorithm to (i) explore the

---

[1] Called « the speed » in the literature, **V** is actually a displacement

solution domain with a high value of ω, (ii) exploit promising areas of the solution domain with a lower value. Then, c_1 and c_2 have to be chosen carefully to optimize the capabilities of the algorithm to converge to the global minimum of the objective function. Moreover, the positions and speeds of the particles have to be constrained for the calculation to converge. The speed is then defined in $[-V_{max}; V_{max}]$, where V_{max} is defined as a function of the solution domain, to be given in the same order of magnitude, such as $V_{max} = (X_{max} - X_{min})/2$ where X_{max} and X_{min} are the extremal values defining the solution domain.

As it has been demonstrated in Di Cesare et al., (2015), the PSO particles can be seen as a Markov chain, and the transition probabilities can be seen as the influence of the particles on each other. The transition probability matrix can then be recalculated at each iteration of the optimization process, by considering the particles' respective performance regarding the best one as the steady-state of the Markov chain to be fitted. In a previous work Di Cesare et al., (2015) , this inverse PageRank-PSO algorithm has been proposed, using the PageRank – an artificial intelligence algorithm used by the world famous search engine Google – to redefine the influences of all the particles on all the others at every iteration of the optimization process. The PSO equations are then modified in the following way:

$$V_i^{t+1} = \omega \times V_i^t + c_1 \times r_1 \times \left(P_{i,best}^t - X_i^t\right) + c_2 \times r_2 \times \sum_{j=1}^{n} C_{ij} \times \left(P_{j,best}^t - X_i^t\right)$$

$$X_i^{t+1} = X_i^t + V_i^{t+1}$$

where **C** is the transition probability matrix, defined by the inverse PageRank algorithm, and defining the influence of all the particles on the others.

The Inverse-PageRank-PSO algorithm has been used in this work to identify the constitutive parameters of the flexural rigidity model of the fishing net.

3.2 Choice of variables to optimize

The numerical model described in previous sections is driven by a set of variables representing the mechanical and dimensional properties of the tested netting material: axial rigidity k, flexural rigidity EI, length of the bar used to model the physical knot, mesh side length and rest angle (half mesh angle when the mesh is free of load), twine weight and the amount of twines contained in a knot.

Some of these variables have been determined by simple measurements or approximations. This choice reduces the complexity of the optimization step and avoids potentially negative angles or distance (De La Prada and Gonzalez, (2015); Sala et al., (2007)). Mesh side length has been measured as the distance between the centers of two adjacent knots. An averaging process is described in the experimental protocol. Linear axial rigidity can be measured through a "stress-strain" experiment. Alternatively, the approximation proposed in section 2.4.1. has been used in the present work. Twine linear weight is a known characteristic supplied by the net maker, known as the twine "runnage". It has been weighed as detailed in the experimental protocol. The amount of twine contained in a knot is needed to calculate the weight of a netting piece. We have used the netting "braiding factor"

approximately equal to $1 + \dfrac{8D}{c}$ where D is the twine diameter and c in the mesh side (Prado, J.;Dremière, (1988)).

Other variables have been identified: the length of the bar used to model the physical knot could be set to 3 times the twine diameter (Prado, J.;Dremière, (1988)). However, physical knots are not symmetrical, their shape depends on twine angle. Thus this variable has been identified through the optimization process. Morvan has measured the rest angle of a piece of netting put on a horizontal vibrating table to ensure that friction forces have a negligible effect. Taking into account the plasticity effects, we assume that the rest angle cannot have a constant value and cannot be measured at rest before deformation cycles, as a traction experiment will definitely modify the shape of the netting model. Thus the rest angle has been identified by the optimization process. EI has also been identified.

The flexural rigidity, the length of the bar used to model the physical knot and the rest angle are defined as the design variables to be identified through the optimization process.

3.3   Numerical test case and effects of discretization

3.3.1   Size of the test case

The test problem is chosen to be easily reproduced by a physical experiment. By knowing the possible variation of dimensional characteristics of netting material, the test case used has 3 meshes in the normal direction and 6 meshed in the transverse direction.

De La Prada and Gonzalez, (2015) used a netting section of 3 x 8 meshes and Morvan et al., (2016) used a section of 5 x 10 meshes. In section 4.1 it is shown that experimental results are reproducible with different netting sections taken on the same netting panel or sell unit.

In order to simulate the physical netting model, the 3x6 virtual meshes model is suspended vertically to a horizontal support, where the 3 upper nodes are free to move only in the support direction with no friction (Fig. 8). Different vertical forces are applied to the 3 lower nodes to model the effect of calibrated weights that will stretch the net during the experiment. The length of the model is defined by the average distance between upper nodes and lower nodes and its width is defined by the average distance between left nodes and right nodes.

3.3.2   Discretization effects

The choice for the sample model discretization is a compromise between accuracy of equations resolution, particularly the calculation of twines curvature radius, and the complexity of the calculation. Six different mesh discretization are compared for PE4x40 samples: 3, 4, 6, 8, 12 and 20 bars per mesh side. Calculated values of Heights (Hi) and Widths (Wi) for weight i (see Table 2) are shown on Fig. 7. One can observe a rapid convergence to a nearly constant value for discretization finer than 6 bars. For each discretization, Table 1 shows the sample width and height relative

differences with the finest discretization values. Compared to the finest discretization, the 6 bars discretization leads to a maximum difference of -4.34% (width) and 2.5% (height) which seems a reasonable compromise. Consequently, the discretization level has been set to 6 bars and the all presented results are obtained with this mesh side discretization.
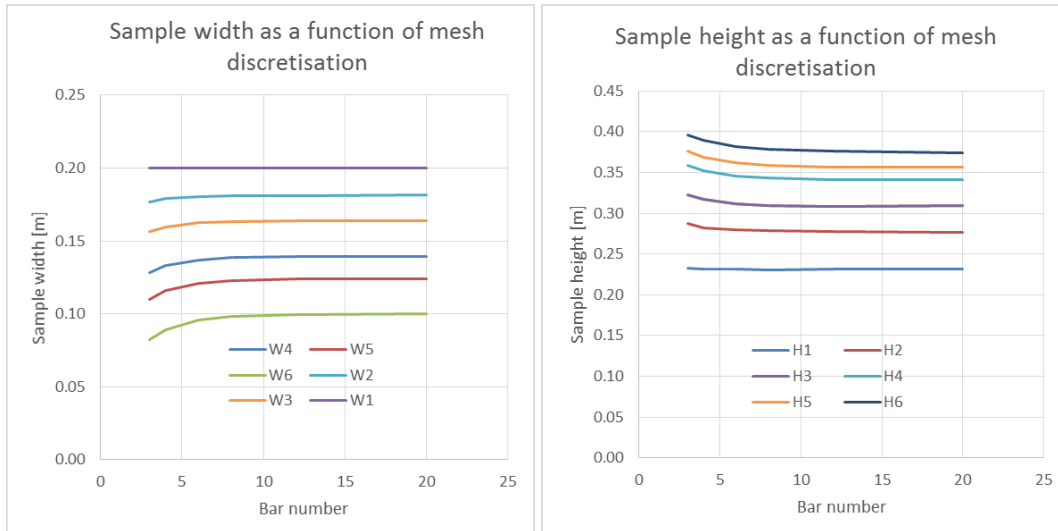

Fig. 7 : calculated width Wi and height Hi for different loads as a function of the discretization.

Number of bars	H1	W1	H2	W2	H3	W3	H4	W4	H5	W5	H6	W6
3	0.48	-0.10	3.79	-2.53	4.56	-4.46	5.40	-8.11	5.78	-11.54	5.74	-17.94
4	0.39	-0.05	2.06	-1.32	2.52	-2.32	3.29	-4.52	3.59	-6.30	4.06	-10.90
6	0.26	0.00	1.08	-0.66	0.94	-0.79	1.38	-1.65	1.63	-2.50	2.03	-4.34
8	-0.17	0.10	0.61	-0.39	0.29	-0.18	0.65	-0.57	0.79	-0.97	1.10	-1.97
12	0.30	-0.10	0.40	-0.22	-0.06	0.12	0.15	0.00	0.22	0.00	0.40	-0.53
20	0.00	0.00	0.00	0.00	0.00	0.00	0.00	0.00	0.00	0.00	0.00	0.00

Table 1 : relative difference (%) between Hi (Wi) with the finest discretization

3.4   Experimental protocol

The netting samples dimensional characteristics were measured with a sliding caliper and a mm scale. Twelve twines (6 meshes in the T direction) were set together side by side on a plane and the average diameter was measured as the sample thickness. This measurement was repeated 6 times per sample for the 3 meshes in the N direction, thus each twine of the sample was taken into account. Notice that the measured diameter is not used in the calculations. Average mesh length was calculated from the measurement of 6 aligned mesh sides, between 2 knot centers (6 measurements per sample of 3 x 6 meshes). Uncertainties were deduced from min and max values.

The experimental setup (Fig. 8) was made of a netting sample with 3 meshes set horizontally and 6 meshes set vertically. Normal netting direction was horizontal and transverse direction was vertical. The 3 upper meshes were linked to 3 hooks that were manually moved on the horizontal support to set them vertically. This prevents the induction of transversal force components to the netting sample.

The netting sample was stretch using lead weights. In order to apply uniform loads on the lower 3 knots, each weight was eventually adjusted by removing some lead with a small diameter drill. The weights were checked using a calibrated balance PE6000 Mettler Toledo. The maximum uncertainty of weights value is 0.4 gr. Six different charges were set to the 3 lower knots to stretch the netting sample, the mass in grams of the weights are shown in Table 2:

Load number	W1	W2	W2	W4	W5	W6
Mass [gr]	0	144.6	300.5	605.4	906.0	1735.0
Total load [N]	0	1.43	2.99	5.94	8.89	17.02
Load per mesh [N]	0	0.477	0.983	1.980	2.963	5.677

Table 2 : applied loads, number, mass and weight in newton

The maximum weight value has been determined so as to produce the maximum stretch of the netting section, due to flexural deformation. Larger weights lead to axial elongation and the model width does not decrease significantly. No pre-loading stage is processed, except the one applied during the netting manufacturing process. Two samples of each netting type were tested. Their characteristics are detailed in Table 3.

Plasticity effects were studied through a series of charge and discharge cycles. For each cycle, the following operations were performed on the experimental setup for each of the 6 loads W1 to W6 and then for the 5 loads from W5 to W1 as follows:

1. Set the charge at the 3 lower knots
2. Move the hooks to ensure that there is no transversal load on the upper knots
3. Wait 50 min and periodically check hooks are still vertical, otherwise move them accordingly
4. Measure the 3 distances between the upper and lower knots, 2 by 2, and calculate the average height
5. Measure the 6 distances between the left and right knots, 2 by 2, and calculate the average width
6. Go to step 1 using next charge case or go to next cycle if unload is finished

Distances were measured with a mm precision ruler. The estimated measurement uncertainty is ± 1 mm.

The duration of 50 minutes has been chosen to ensure that the sample reached an almost constant height so that the plastic deformation is taken into account. The criterion used was the height increased/decreased by less than 1% in a 10 minutes interval.

Cycles were repeated until the experimental protocol produces repeatable height and width measurements with a maximum relative difference of 3% on the height. Following this criterion, we observed that the cycles 3 and 4 were reproducible. Heights (widths) are then averaged for the cycles 3 and 4 for each weight. The lengths measured in the load process are averaged with the lengths measured in the unload process. Finally, for each load, measured deformations for the 2 samples are

averaged to be used in optimization process in the objective of suppling the end user with averaged nettings characteristics.
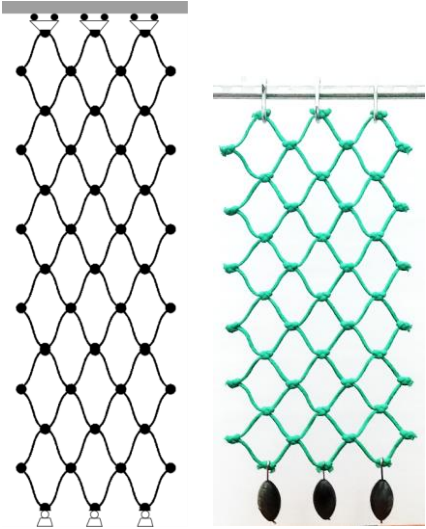

Fig. 8 : experimental setup made of a 3x6 meshes piece of netting. The model is set with normal direction horizontally and transverse direction vertically (so-called T90 usage). The 3 upper nodes are free to move in the horizontal direction and blocked in other directions.

4 Results

4.1 Experimental results

Three different netting types have been studied (Table 3). Measured heights and widths for the 4 load/unload cycles are presented on Fig. 9 for PE4 40. Graphics for other nettings and detailed values are presented in the Supplementary material. The maximum relative height difference between cycles 3 and 4 is 2.16% for PE4x40 sample.

Sample designation and material	Diameter [mm]	Avg Mesh side [mm]	Sample number and Sample size [mesh number N x mesh number T]	Avg. sample mass [kg]
Green polyethylene PE3 40	2.6±0.1	39.33±0.3	2 sample of 3x6 meshes	0.0191
Green polyethylene PE4 40	3.7±0.2	38.83±0.3	2 sample of 3x6 meshes	0.0265

Green polyethylene PE4 60	3.4±0.2	60.80±0.5	2 sample of 3x6 meshes	0.0365

Table 3 : tested netting dimensional characteristics and mass
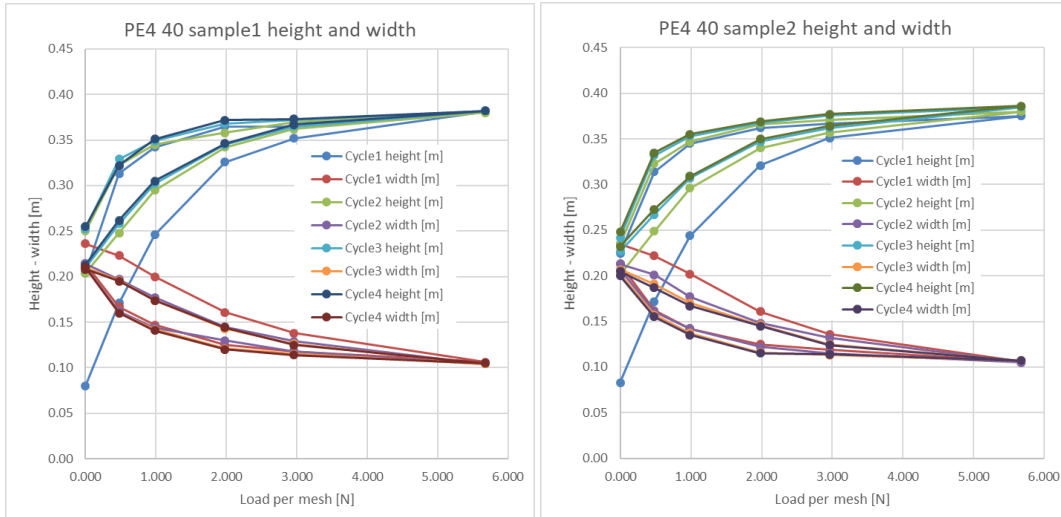

Fig. 9 : measured heights and widths for different loads on PE4 40, sample 1 and sample 2
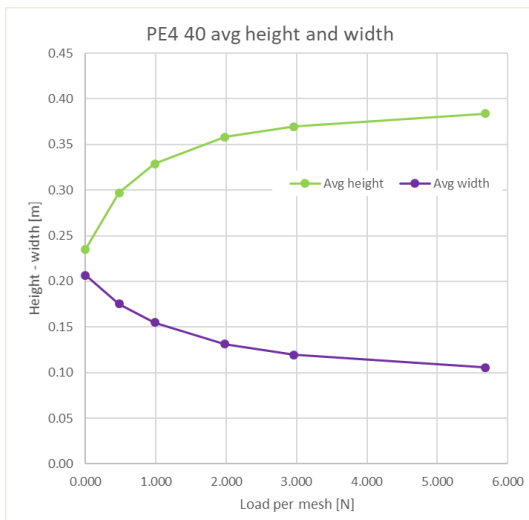

Fig. 10 : Averaged measures (sample 1 and sample 2 for cycles 2 and 3) for the different loads

4.2   Inverse identification results

Heights and widths presented in Fig. 10 are used to identify EI, the rest angle and the length of the virtual knot for PE4 40 netting. The quality of the identification is tested through the standard determination coefficient R² and the mean absolute percentage error (MAPE):

$$R^2 = \frac{1}{N} \frac{\sum (y_i - \hat{y}_i)^2}{\sum (y_i - \bar{\bar{y}})^2} \qquad MAPE = \frac{100}{N} \sum \left| \frac{y_i - \hat{y}_i}{\hat{y}_i} \right|$$

Where $\hat{y}_i$ are the experimental points (the objectives of the optimization) and y_i are the simulated points. $\bar{\bar{y}}$ is the average objective. During the optimization process, MAPE was used to calculate the error function.

The parameters of Inverse-PageRank PSO are the following: $c_1 = c_2 = 2$ and ω is linearly decreasing from 0.8 to 0.4 as the iterations are going. The boundaries of the design domain are defined separately for each design variable as given in Table 4, and the extremal particles' displacements are defined as 20% of these design domains.

	Extrema position
Angle [°]	[0;70]
Stiffness [N/m2]	[1e-5 ;1e-3]
Knot length [mm]	[0.002 ;0.015]

Table 4 : Design domain definition

Table 5 shows the identified values for the 3 parameters for the different tested nettings and Fig. 11 shows the simulation results with identified parameters compared to experimental results.

	EI [N/m²]	Angle [°]	Knot length [mm]	R^2	MAPE%
PE3x40	4.30E-05	33.50	5.34	0.9968	2.69
PE4x40	8.66E-05	32.4	5.02	0.9957	2.27
PE4x60	8.84e-05	40.21	8.86	0.9986	2.08

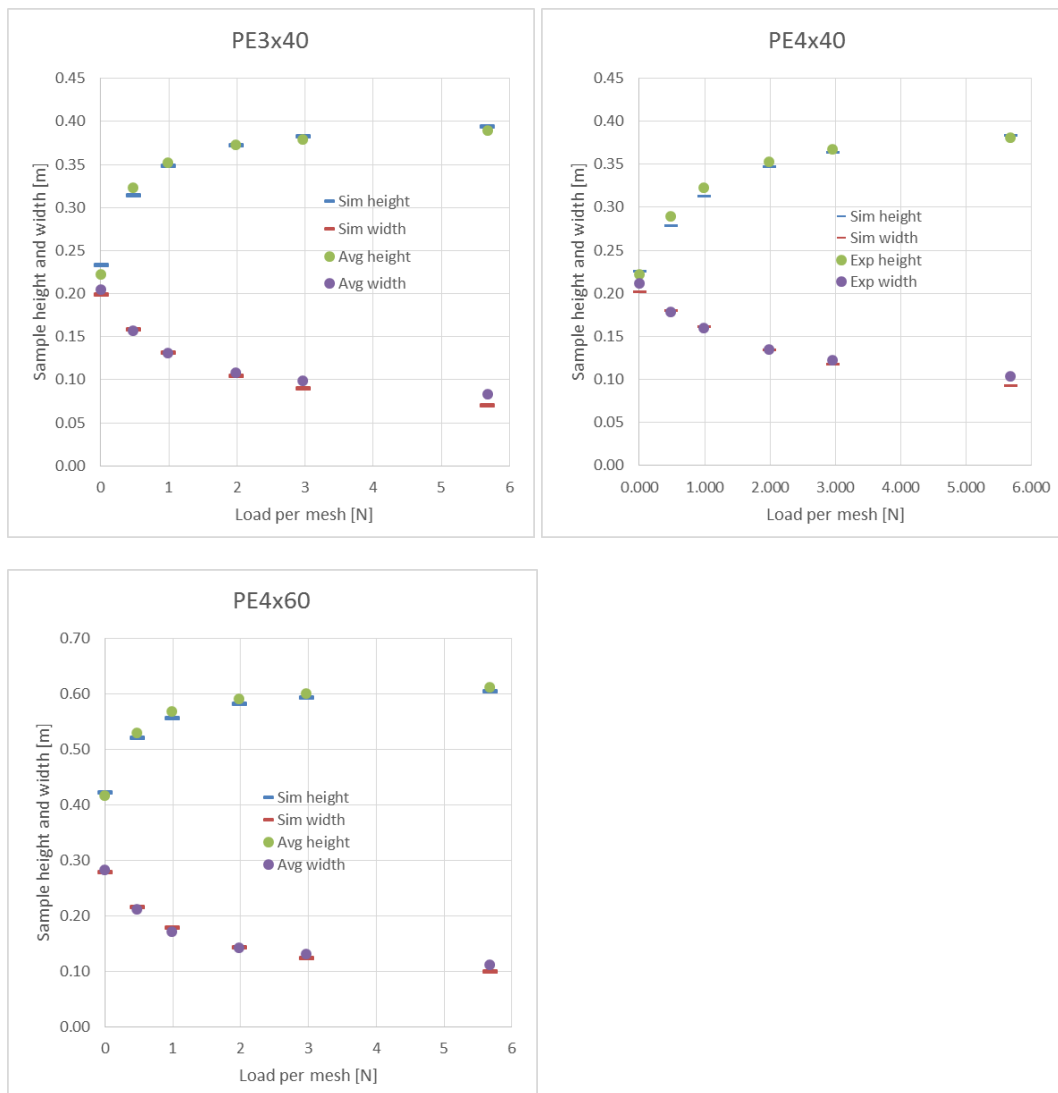Table 5 : optimization results for PE3x40 PE4x40 and PE4x60

Fig. 11 : Simulation with optimal parameters and experimental results for PE3x40, PE4x40 and PE4x60

4.3 Comparison with other author's results

The current methodology was applied to identify parameters from experimental results established by Morvan Morvan et al., (2016) with a different experimental protocol. The author measured the vertical elongation of netting sample made of different materials (

Table 6).

| Material and designation	Diameter [mm]	Mesh side [mm]	Sample number and Sample size [mesh number N x mesh number T]	Average mass sample [kg]

Green polyethylene PE4x40_b	3.14	40.44	10 samples of 4x10 meshes	0.0618
Double twine green polyethylene DPE4x50_A	3.14	49	5 samples of 4x10 meshes	0.164
Double twine green polyethylene DPE4x50_B	3.14	49	5 samples of 5x25 meshes	0.486
Breztop polyethylene BTPE2.5x40	2.5	40	10 samples of 4x10	0.0184
Brezline polyethylene BLPE4x60	4	59.84	10 samples of 4x10	0.1176

Table 6 : description of samples used by other authors. Brezline and Breztop are trademarks of LE DREZEN Company.

The two main differences between the experimental protocols used by Morvan and the one used in the present work are (1) the measurement of the rest angle on the sample at rest on a vibrating table to remove friction effects vs. the identification of the rest angle in present work and (2) no particular care to take into account plasticity effects vs. the use of the last repeatable cycles after several load / unload cycles in the present work. This last difference can be the cause of differences between parameters identified in the present work experiments and Morvan's experiments. Moreover, 10 samples of each material where tested by the author.

An important modeling difference comes from the node length: it is not taken into account by Morvan (there is no virtual knot) while it is taken into account in the present work

The 3 variables (EI, angle at rest and node length) have been identified with a 6 bars model from the average elongation of all samples for each load. Measured average samples and calculated elongations with the optimized parameter are shown in Fig. 12.
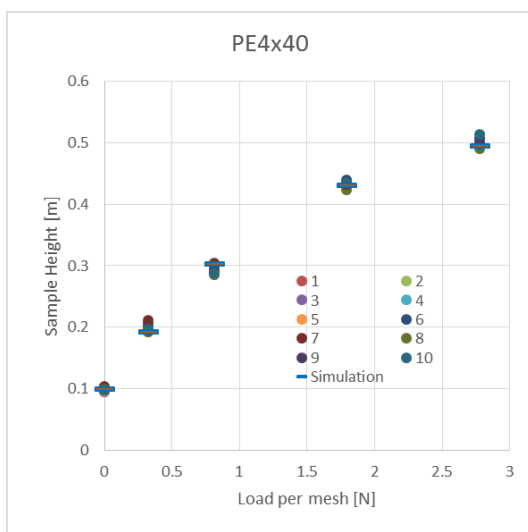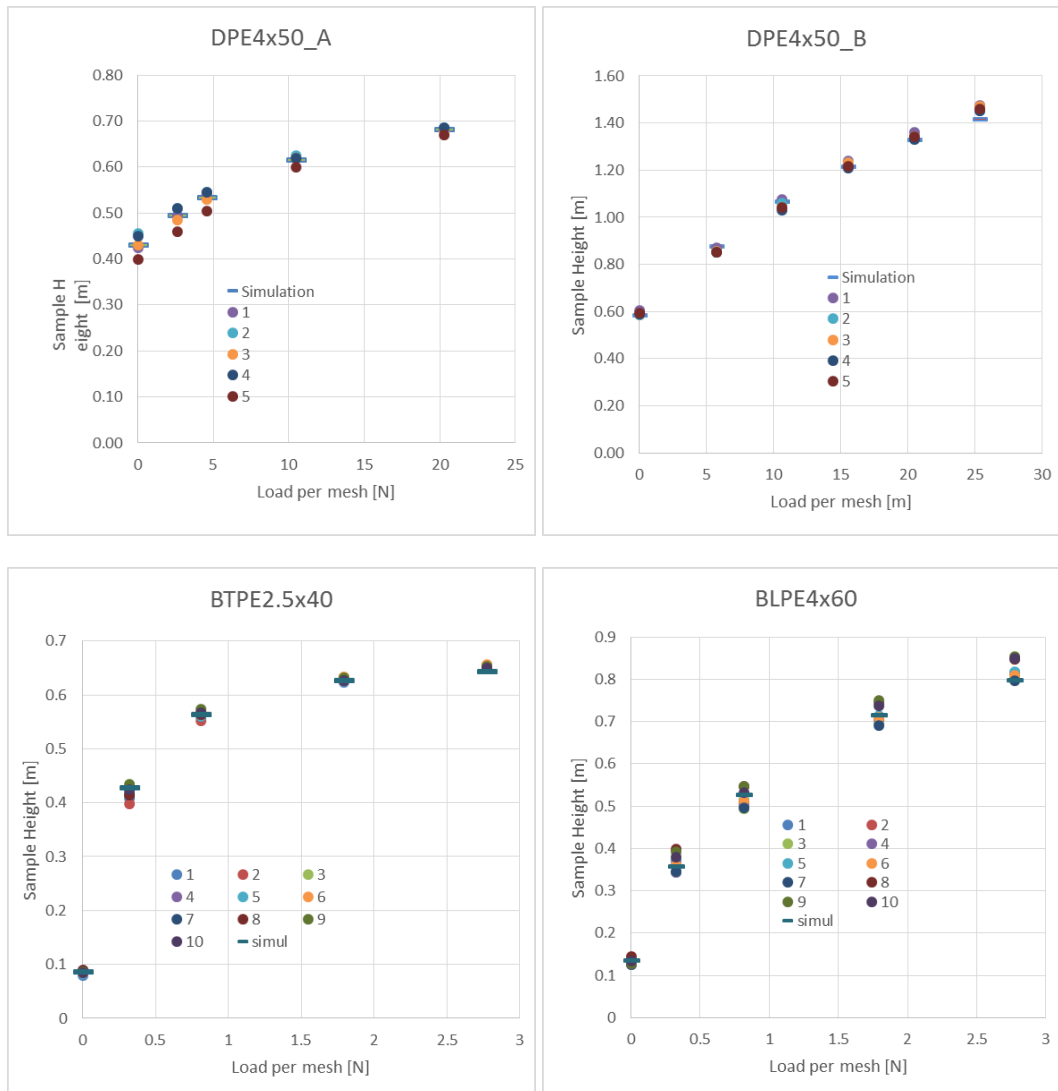
Fig. 12 : sample elongation as a function of load per mesh, experimental results (points) and calculation results for optimal parameters set.

Table 7 summarizes the results and shows the values of identified parameters. Roughly we can observe EI values are smaller for present methodology, as expected

	Present work results			Morvan results	
	R²	EI [N/m²]	Rest angle [°]	EI [N/m²]	Rest Angle [°]
PE4x40_b	0.998425	8.07E-05	7.08	1.80E-04	7.00
DPE4x50_A	0.999522	3.22E-04	30.7	6 to 8e-4	24.29
DPE4x50_B	0.994542	3.88E-04	12.9	6 to 8e-4	24.29
BTPE2.5x40	0.999312	1.71E-05	1.35	3.5 to 5.5e-5	6.13
BLPE4x60	0.997388	1.30E-04	0.68	2.5 to 3.5e-4	6.32

Table 7 : Optimization results from other authors experiments

De La Prada and Gonzalez, (2015) have studied different netting materials. One sample of 4x8 meshes for each netting. It cannot be stated that fibers constituting twines are the same than the one used in present work. Measured heights and widths are not detailed, thus identification using present method cannot be undertaken from her measurements. Moreover, she has presented different results derived from different modelling, with or without optimization parameters constraints and the parameters were identified separately for the load and unload processes. De La Prada results with min/max constrain on all parameters and present work results are compared in Table 8.

	Present work results			De La Prada results			
	R²	EI [N/m²]	Rest angle [°]	EI [N/m²]	Rest Angle [°]	R²	
PE3x40	0.9968	4.30E-05	33.5	3.4 to 5.7 e-5	7 to 15	0.9931 to 0.9984	loading
				1.2 to 3.1 e-5	44 to 50	0.9635 to 0.9903	unloading
PE4x40	0.9957	8.66E-05	32.4	6.6 to 11.9 e-5	15 to 19	0.9949 to 0.9996	loading
				2.2 to 4.2 e-5	44 to 50	0.9860 to 0.9930	unloading

Table 8 : comparison for PE3x40 and PE4x40 with other author's results, loading and unloading cycles

4.4 Sensitivity analysis

The value of each of the three variables (flexural rigidity, mesh angle at rest, knot length) is separately increased by 10% from its optimal value to assess the effect on the calculated sample width and height for each load. This can be interpreted as assessing the error on geometry parameters (samples width and height) resulting from an identification error of a driving parameter.

EI, the rest angle and the node length are increased by 10% from their respective optimal values. Errors on height and width, and maximum errors observed are given in Table 9.

Charge [N]	EI		Rest angle		Node length	
	errHeight [%]	errWidth [%]	errHeight [%]	errWidth [%]	errHeight [%]	errWidth [%]
0.00	-0.50	0.14	8.28	-1.97	-2.48	0.33
1.42	-1.94	2.02	2.52	-2.61	-3.03	1.94
2.95	-1.55	3.34	1.37	-2.36	-2.74	2.95
5.94	-0.83	3.89	0.79	-2.39	-2.55	4.13
8.89	-0.42	3.13	0.58	-2.26	-2.38	4.38
17.02	-0.19	2.64	0.32	-1.72	-2.33	5.64
Max. error [%]	3.9		8.3		5.6	

Table 9 : effect on height and width of a 10% overestimation of EI

4.5   Application to the simulation of netting tubes shape

Two tubes were built from PE4 40 and PE3 40 netting. Each tube has 29 meshes in circumference and is 35 meshes high. So as to ensure the circular shape continuity, knots of each sides were welded together two by two. Each tube was attached to a horizontal rigid 65 cm diameter circular frame with regular spacing between knots. The protocol used to assess the load-geometry relation was similar to the one described in 0 : the total load (among 0N, 8.84N, 20.15N, 30.03 N, 41.91N) was attached to the lower knots. After a period of 50 minutes, the following characteristics were measured with a mm ruller:

- Average height,
- Minimum diameter at the neck of the tube
- Distance from the upper part of the position of the minimum diameter
- Average diameter of the lower part of the tube,

Heights and diameters were measured 3 times (at 120°) and averaged. The first cycles were ignored until repeatable geometrical characteristics could be measured.

The simulations were achieved with the 6-bars model. Fig. 13 shows the measurement and simulation results with identified parameters for each netting.
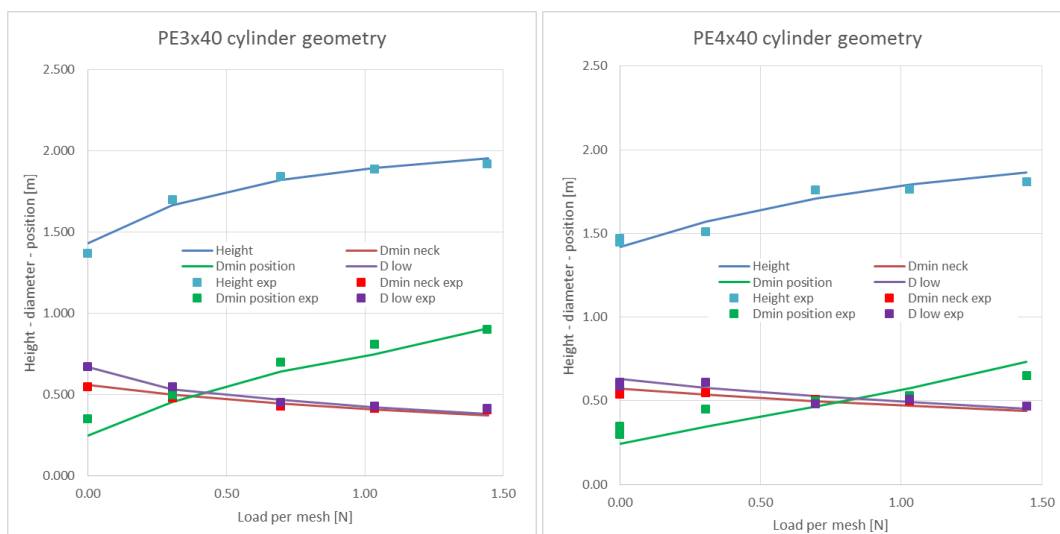

Fig. 13 : PE3 40 and PE4 40 netting tubes. Measured height, diameter and position of minimum diameter [m] as a function of the load per mesh [N] (points) and simulation (lines).
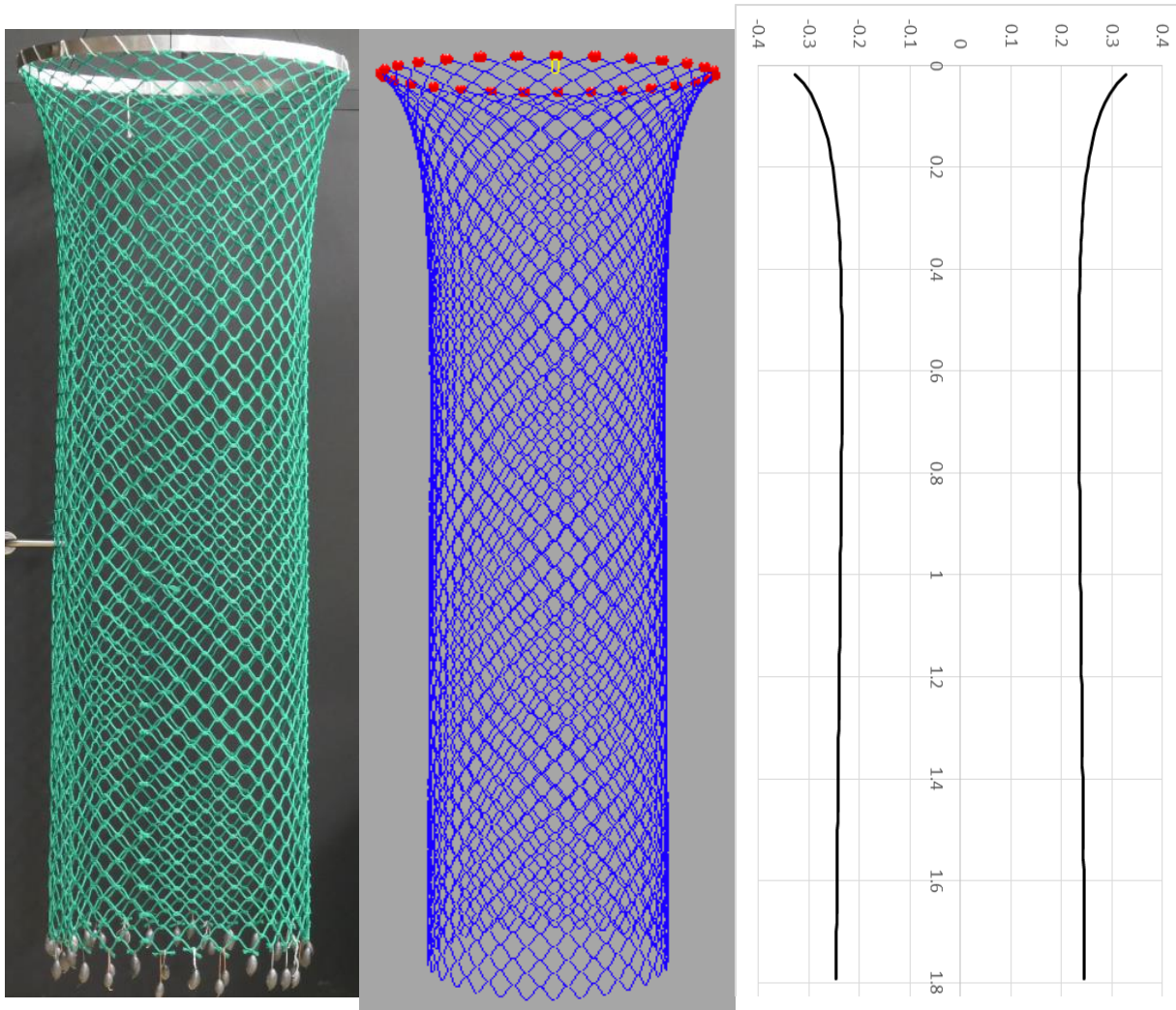
Fig. 14 : PE4 40 netting tube under the load of 1.04 N per mesh. From left to right, photo taken during experiment, 3D view of the simulation result, simulated profile in a symmetry plane.

Results provided by the model are in reasonably good agreement with measures for height and diameters. Large relative errors were sometimes found for the position of the tube neck. It must be noticed that the cylinders are not perfectly symmetrical, due to the welding process and inhomogeneous netting. This brings to measurement uncertainties. Moreover, this result can be explained by the difficulty to accurately measure the neck position.

5   Discussion

This article presents a new method to identify flexural rigidity, rest angle, knot length and enables the simulation of large deformation of nettings constructions including 3D flexural rigidity. The two-dimensional flexural rigidity EI has already been addressed in previous studies (De La Prada, 2014; De La Prada and Gonzalez, 2015; De La Prada and González, 2016; Morvan et al., 2016), as well as the mesh angle at rest (De La Prada and Gonzalez, (2015); De La Prada and González, (2016)). The length of the physical knots has been added taking into account plasticity effects.

Present method was applied to the set of experimental data of Morvan et al., (2016), where the netting knots length is null and identification results were compared. The stretch mesh length being the same in both approaches, mesh sides (excluding the knot length) are then slightly shorter when modeling a virtual node in the present work. Consequently, we could anticipate over estimated EI values for Morvan: his mesh sides being longer, higher EI values leads to the sample height for a given load. This assumption is verified for each netting type: Morvan's EI values are roughly 2 times greater than values identified by present method on his experimental values. Rest angle has been measured with no load (vs. identified in present work) but values are not significantly different (Table 7). As expected, rest angle value for same netting types are greater for the present work (33.5° vs. 7° for PE4x40 and 40.21° vs. 6.32°). Taking plasticity effect into consideration, identified EI value for PE4x40 and PE4x60 using present experimental protocol (respectively 8.66E-05 and 8.84E-5 N/m²) are expected to be smaller than Morvan's values. Indeed, the sample heights for load/unload cycles 3 and 4 are greater than for a single cycle (Morvan's protocol). This assumption is also verified.

Identified parameters for PE3x40 and PE4x40 were compared to De La Prada and Gonzalez, (2015) results. The comparison is easier as the methodologies are closer. The two methods differ by a separate identification for load and unload and by different (constrained, unconstrained parameters) optimization approaches. Results are quite comparable: EI and mesh angle at rest for the present work are inside the extrema depending on the modeling method used by the author, averaged De La Prada EI (load and unload, min/max constrain) for PE3x40 is 3.35E-05 N/m² (vs. 4.30E-05) and 6.22E-05 N/m² for PE4x40 (vs.8.66E-05). Average angle at rest is 29° (vs.33.5°) for PE3x40 and 32° (vs. 32.4°) for PE4x40.

EI values for different mesh sides with same twine diameter should be close. In the case of 4mm diameter netting, this assumption is verified in present work (8.66E-05, 8.84E-5 N/m², 2% difference) but is not verified for Morvan's 4mm samples (8.07E-05, 3.22E-04, 3.88E-04, 1.30E-04 N/m²). Furthermore, inertia varies with the 4th power of the diameter. The ratio between EI (4mm) and EI (3mm) is around 2 in present work and for averaged De La Prada values, but is expected to be around 3.2 (around 3.3 when considering measured diameters). Possible characteristic dispersion of the fibers constituting the different twines, twine diameter reduction when load increases could explain this result.

The number of samples (2 samples in present work compared to 1 sample studied by De La Prada and 10 or 5 (double twine) samples studied by Morvan) and the size of each sample (3x6 meshes for each netting vs. 4x8 meshes for De La Prada and 4x10 or 5x25 (double twine) meshes for Morvan) does not seem to have a major influence on EI results: less than 5% variation for the 10 samples of Morvan). It

confirms our choice for sample number and size. It also confirms our choice to consider the average height and width values for each sample pair. Moreover, identified values applied to larger netting structures (cylinders made of 29 meshes in circumference and is 35 meshes height) lead to calculated cylinder heights that compare with experimental values with MAPE errors of 2.98% for 4x40 cylinder and 1.92% for 3x40 cylinder.

Nevertheless the identified node length (5.34 5.02 and 8.86 mm respectively for PE3x40 PE4x40 and PE4x60) differ from expected values, about 3 times the diameter (De La Prada and Gonzalez, (2015); Prado, J.;Dremière, (1988)). This can be interpreted as an attempt to optimize driving parameters so as to compensate imperfect mechanical model, for instance plasticity which is not modelled.

The capacity of the developed model to reproduce experimental data is not perfect (R^2 <0.999, MAPE>2%) especially with larger loads. This can be explained by (1) modeling hypothesis: the twines diameter is supposed to be constant but it decreases when tension increases; friction among fibers constituting twines is not taken into account, thus EI is not constant as it has been shown by Morvan et al., 2016 :EI varies by less than 6% for single twine PE and less than 10% for other materials with larger variations for lowest loads. (2) The model does not take into account plasticity effects and consequently cannot not reproduce them. Thus, when averaging load and unload cycles, the resulting optimization objectives become more difficult to fit. In the same way, the number of objectives has been increased with the measured sample width, which reduces the possibility to perfectly fit them. However, the precision observed for cylinder models (MAPE<3%) makes this methodology a good candidate for fisheries applications by taking into consideration the uncertainties of nettings and fishing gear characteristics.

A rapid sensitivity study has shown that the more sensitive variable is the mesh angle at rest but however with no amplification effect: the output model uncertainty remains lower than the angle uncertainty. In the meantime, there is a lack of unified methodology among different authors to identify the mesh rest angle.

Future work should consider the plasticity in the modeling and a more realistic model for the netting knot: the way twines are embedded in an actual knot is different for the 4 twines, knots are not symmetrical and their shape change with the mesh load. This could lead to improve of the experimental protocol. Studying artificially aged netting materials could be complementary to the plasticity study. Taking into account twine torsion effects are also potential improvements for better understanding and implementation of netting structures simulation.

References

Bessonneau, J.S., Marichal, D., 1998. Study of the dynamics of submerged supple nets (application to trawls). Ocean Eng. 25, 563–583.

De La Prada, A., 2014. Efficient and accurate methods for computational simulation of netting structures with mesh resistance to opening. Thèse.

De La Prada, A., Gonzalez, M., 2015. Quantifying mesh resistance to opening of netting panels: experimental method, regression models, and parameter estimation strategies. ICES J. Mar. Sci. 72(2), 697–707. https://doi.org/10.1038/278097a0

De La Prada, A., González, M., 2016. Nonlinear stiffness models of a net twine to describe mesh resistance to opening of flexible net structures. Proc. Inst. Mech. Eng. Part M J. Eng. Marit. Environ. 230, 33–44. https://doi.org/10.1177/1475090214530876

Di Cesare, N., Chamoret, D., Domaszewski, M., 2015. A new hybrid PSO algorithm based on a stochastic Markov chain model. Adv. Eng. Softw. 90, 127–137. https://doi.org/10.1016/j.advengsoft.2015.08.005

Herrmann, B., Wienbeck, H., Moderhak, W., Stepputtis, D., Krag, L.A., 2013. The influence of twine thickness, twine number and netting orientation on codend selectivity. Fish. Res. 145, 22–36. https://doi.org/10.1016/j.fishres.2013.03.002

J. Kennedy;R. Eberhart, 1995. Particle swarm optimization, in: Proceedings of the Annual International Conference of the IEEE Engineering in Medicine and Biology Society, EMBS. pp. 6556–6559. https://doi.org/10.1109/IEMBS.2011.6091617

Le Bris, F., Marichal, D., 1999. Numerical and experimental study of submerged flexible nets: Applications to fish farms. Proc. 1999 Ninth Int. Offshore Polar Eng. Conf. (Volume 3), Brest, Fr. 30 May - 4 June 1999 749–755. https://doi.org/10.1007/BF02492931

Morvan, B., Priour, D., Guede, Z., Bles, G., 2016. Finite element model for the assessment of the mesh resistance to opening of fishing nets. Ocean Eng. 123, 303–313. https://doi.org/10.1016/j.oceaneng.2016.07.026

Nguyen, T.X., Winger, P.D., 2016. Numerical Modeling - A Comparison of Different Methods for Simulating Bottom Trawls. Fish. Technol. 53, 9–29.

Nguyen, T.X., Winger, P.D., Orr, D., Legge, G., Delouche, H., Gardner, A., 2015. Computer simulation and flume tank testing of scale engineering models: How well do these techniques predict full-scale at-sea performance of bottom trawls? Fish. Res. 161, 217–225. https://doi.org/10.1016/j.fishres.2014.08.007

O'Neill, F.G., 2002. Bending of twines and fibres under tension. J. Text. Inst. 93, 1–8. https://doi.org/10.1080/00405000208630548

Prado, J.;Dremière, P.Y., 1988. Guide pratique du marin pêcheur, Tec & Doc. ed.

Priour, D., 2001. Introduction of mesh resistance to opening in a triangular element for calculation of nets by the finite element method. Commun. Numer. Methods Eng. 17, 229–237. https://doi.org/10.1002/cnm.398

Priour, D., Cognard, J.-Y., 2011. Investigation of methods for the assessment of the flexural stiffness of netting panels, in: DEMaT'11.

Reynolds, C.W., 1987. Flocks, herds, and schools: A distributed behavioral model. Proc. 14th Annu.

Conf. Comput. Graph. Interact. Tech. SIGGRAPH 1987 21, 25–34.
https://doi.org/10.1145/37401.37406

Robertson, J.H.B., Stewart, P.A.M., 1988. A comparison of size selection of haddock and whiting by square and diamond mesh codends. ICES J. Mar. Sci. 44, 148–161.
https://doi.org/10.1093/icesjms/44.2.148

Sala, A., O'Neill, F.G., Buglioni, G., Lucchetti, A., Palumbo, V., Fryer, R.J., 2007. Experimental method for quantifying resistance to the opening of netting panels. ICES J. Mar. Sci. 64, 1573–1578.
https://doi.org/10.1093/icesjms/fsm113

Wanchana, W., Kanehiro, H., Inada, H., 2002. Fatigue property of high-performance polyethylene netting twine. Fish. Sci. 68, 371–379.